Research Article

Ziliu Xiong*, Zhangguo Lin, Jianjun Qi, Li Sun, Guangxin Wu, Shuang Kuang, and Guoping Zhou

Research on high-temperature oxidation resistance, hot forming ability, and microstructure of Al-Si-Cu coating for 22MnB5 steel

https://doi.org/10.1515/htmp-2021-0040 received June 04, 2021; accepted October 14, 2021

Abstract: High-temperature oxidation resistance, hot formability, element distribution, and microstructure of Al-10% Si-(0.5–3.0%)Cu coating were investigated by means of glow discharge spectroscopy, optical microscope, scanning electron microscope, and energy-dispersive spectroscopy. Results show that the addition of Cu can increase high-temperature oxidation resistance above 950°C and improve hot formability so that no crack spreads into substrate steel as hot forming at 33.3% strain. Oxidation film structure is continual and compacting, and Si highly concentrates in the surface layer. The distribution of Cu has skin effect with peaking content 8.2% in the surface layer. After hot stamping, Al and Si diffuse into substrate steel, and Cu diffuses from inner to outer coating. Al–Si–Cu coating has

smoother surface, straighter diffusion layer, and finer metal compound than Al–Si coating. Surface and diffusion layers are identified as aluminum oxide, Si-rich, and Cu phase and Al₇SiFe₂, Al₃Fe, and CuAl₃, respectively. Al-rich phase and the metal compound are composed of α -Al dissolving Fe, Si, and Cu and Al–Si matrix, Cu₃Al, respectively.

Keywords: Al–Si–Cu coating, 22MnB5 steel, high-temperature oxidation resistance, hot stamping ability

1 Introduction

Hot-forming technology was developed in 1970s in Europe and, first, successfully applied in side beam manufacture in 1984 [1]. In the process of hot forming, hot-forming steel has high hot stamping ability and ultrahigh strength after quenching, so it is used in automobile manufacturing. So hot forming technology and hot forming steel have received a rapid development in the last 50 years. Hot forming steel is used in car body manufacture with high mass percentage 10–30% nowadays, which is considered to be a better weight reduction material for body in white in contrast to cold forming high-strength steel.

However, hot forming steel also has shown large terms of problems, such as surface oxidation, surface decarburization, and die wear during hot forming process. Therefore, high-temperature resistance coating is invented to protect base steel, such as Al–Si, galvanic iron (GI), and galvanizing iron (GA). High-temperature oxidation resistance and corrosion resistance of coating are critical application performance index of hot forming steel. Low antihigh-temperature oxidation resistance of Al–Si coating will reduce the service life of the furnace roller when the coating melts in the heating process and will also reduce the production efficiency and service life of the hot rolling die in the hot forming process. Hot formed cracks in GI/GA coating may extend to substrate, which will worsen

e-mail: Xiongziliu@hbisco.com, tel: +86-0311-6650-8898

Zhangguo Lin: HBIS Group Technology Research Institute, HBIS Group, Shijiazhuang, 050023, Hebei Province, China,

e-mail: Linzhangguo@hbisco.com

Jianjun Qi: HBIS Group Technology Research Institute, HBIS Group, Shijiazhuang, 050023, Hebei Province, China,

e-mail: Qijianjun@hbisco.com

Li Sun: Automotive Material Research Institute, HBIS Group Technology Research Institute, HBIS Group, Shijiazhuang, 050023, Hebei Province, China, e-mail: Sunli@hbisco.com

Guangxin Wu: State Key Laboratory of Advanced Special Steel, Shanghai University, Shanghai, 200444, China,

e-mail: gxwu@shu.edu.cn

Shuang Kuang: Technology Research Center, HBIS Tang Steel, Tang Shan, 063016, Hebei Province, China,

e-mail: kuangshuang@hbisco.com

Guoping Zhou: High Strength Automotive Steel Co., Ltd, HBIS Tang Steel, Tang Shan, 063016, Hebei Province, China, e-mail: zhouguoping@hbisco.com

^{*} Corresponding author: Ziliu Xiong, Automotive Material Research Institute, HBIS Group Technology Research Institute, HBIS Group, Shijiazhuang, 050023, Hebei Province, China,

Table 1: Chemical components of 22MnB5 (wt%)

Steel	С	Si	Mn	Cr	Ti	В	Fe
22MnB5	0.22	0.30	1.40	0.20	0.04	0.003	Bal

application of hot forming steel. Some research improve the high-temperature oxidation of coating by controlling the heating time and temperature to increase the content of Fe and Fe alloy phase, but this reduces the hot forming ability. Hence, coating with both high-temperature resistance and hot forming ability is needed for hot formed steel.

Therefore, it is necessary to develop a new coating composition, which can improve the high-temperature oxidation resistance of aluminum silicon coating, so as to provide higher protection for steel plate. Unfortunately, few studies in the literature can solve this problem. Tsuru [2] and Kruehong et al. [3] and Takata et al. [4] studied the morphology, corrosion behavior, and alloy layer growth of hot-dip Al-Si-Mg coating. The results show that the addition of Mg can significantly improve its electrochemical properties, but the alloy contains 7-9 wt% Mg and 4-5 wt% Si [2,3], which is unlikely to be applied in industry. Zhang's et al. work [5] describes the hot-dip coating of a novel Al-Si-Mg-Cu alloy on steel, coating characterization and corrosion property evaluation. It is shown that coating has excellent corrosion resistance compared to galvanized steel, whereas the high-temperature resistance has not been studied. Therefore, there is a full opportunity to study the corrosion and properties of aluminum alloy coatings on steel.

In this article, 0.5–3.0 wt% Cu was added to the Al-10% Si coating, and the effects of Cu on the microstructure, high-temperature oxidation resistance, and hot formability of the Al–Si–Cu coating were studied.

2 Materials and methods

The coating is Al-10% Si-(0.5–3.0%) Cu, and the substrate is 22MnB5 and its chemical components are shown in Table 1.

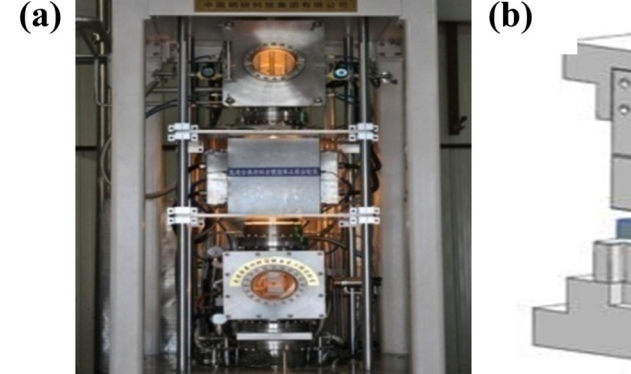
22MnB5 steel sheets with 2 mm thickness were prepared by vacuum melting, hot rolling, acid pickling, and cold rolling process in the lab of HBIS Group Technology Research Institute, and then the steel sheets were cut into samples with a size of 220 mm \times 120 mm.

These samples were treated by acid pickling, alkali washing, degreasing, rinsing, and drying and then were annealed and hot dipped in the hot-dip simulator (Figure 1(a)). The detailed annealing and hot-dip process parameters were as follows: heating up rate 10°Cs^{-1} , heating temperature 850°C, hot-dip temperature 680°C for 8 s, and coating cooling rate 10°Cs^{-1} .

The prepared samples were subjected to heating and hot forming process according to Figure 2. The detailed parameters were as follows: heating rate $10^{\circ}\text{C}\cdot\text{s}^{-1}$, soaking temperature 950°C holding for 60 s, hot forming temperature 700–900°C, and die quenching cooling rate $40-80^{\circ}\text{C}\cdot\text{s}^{-1}$ for holding for 10 s.

High-temperature oxidation experiment of Al–Si–Cu and commercial Al–Si coating sample under different heating temperatures of 650, 750, 850, and 950°C soaking for 2 h were carried out. Then weight-increasing rate of samples was calculated using equation (1). In this article, microstructures of coatings were observed by optical microscope (OM) and OXFORD scanning electron microscope (SEM) after samples were polished and etched with 0.5% hydrofluoric acid.

Element distributions in coatings were tested by glow discharge spectroscopy (GDS) of HJY PROFILER 2. Element contents in different microstructures were studied using energy dispersive spectroscopy (EDS).



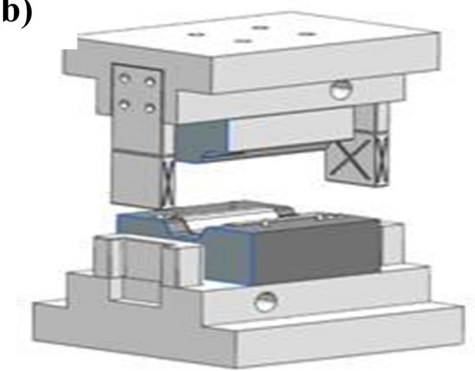


Figure 1: Hot-dip simulator machine and hot forming tooling: (a) hot-dip simulator machine and (b) hot forming tooling.

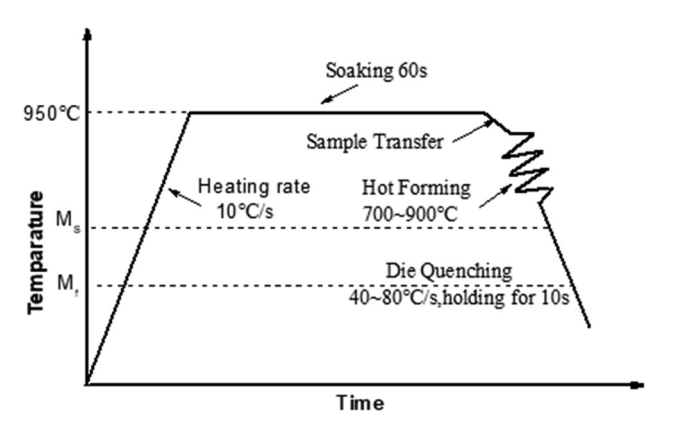


Figure 2: Heating and hot stamping process of Al-Si-Cu coating sample.

Weight increasing rate

$$= \frac{\text{Weight after heating - Weight before heating}}{\text{Surface area} \times \text{Soaking time}}$$
 (1)
$$\times 100\%.$$

3 Results and discussion

3.1 High-temperature oxidation resistance and hot stamping ability

It could be seen that hot-dip coating shown in Figure 3(a) has good surface quality and bright silver color, and that hot stamping coatings shown in Figure 3(b) and (c) have unbroken compacting surface with gray and Cambridge blue color. Comparing surface oxidation of coating and uncoating zones of hot stamping samples, no peeling and scaling defects distribute in the coating zone, but serious oxidation layer and lots of pealing scales show in uncoating the surface zone. There are no forming cracks and defects on the surface of coatings with different forming radii after the hot stamping. Tensile deformations of hot stamping samples with different forming radii are, respectively, 33.3 and

20.0%, calculated by pure bending, as shown in Figure 4. These can be concluded that Al–Si–Cu coating has a perfect hot forming ability even at more than 30% hot forming deformation. By contrast, the hot forming ability of commercial Al–Si coating is so poor that whole coating will crack at more than 30% hot forming deformation with hot forming temperature of 800°C, and Al–Si coating only can be applied for indirect hot forming process [6,7]. These phenomena prove that Al–Si–Cu coating has a perfect high-temperature resistance property, adhesive property, and hot forming ability, which protects basic steel successfully during the process of high heating temperature treatment and big strain hot stamping.

To further evaluate hot forming performance, SEM microstructures of hot-dip coating and hot stamping coatings with forming radius of 2 and 4 mm are shown in Figure 5(a)–(c), respectively. Sampling positions of the microstructures shown in Figure 5 are from white square in Figure 3.

It could be obviously seen that there is no crack in inner microstructure of hot-dip coating. And although there are some cracks in inner microstructure of hot forming coating, there is no any crack throughout basic steel and oxidation film. Hence, it is suggested that increasing hot deformation strain of hot stamping coating from 20 to 33.3% just generates wider cracks in microstructure of coating without breaking coating and compactness of surface oxidation. Moreover, it is also suggested that Al–Si–Cu coating has better hot stamping forming ability than Al–Si coating, which needs precold forming to get the same effect [6].

3.2 High-temperature resistance and hot forming ability

3.2.1 Evaluation of high-temperature resistance

Coating morphology and oxidation weight increasing rate curve of Al–Si–Cu coating are shown in Figure 6(a) and (b), respectively.

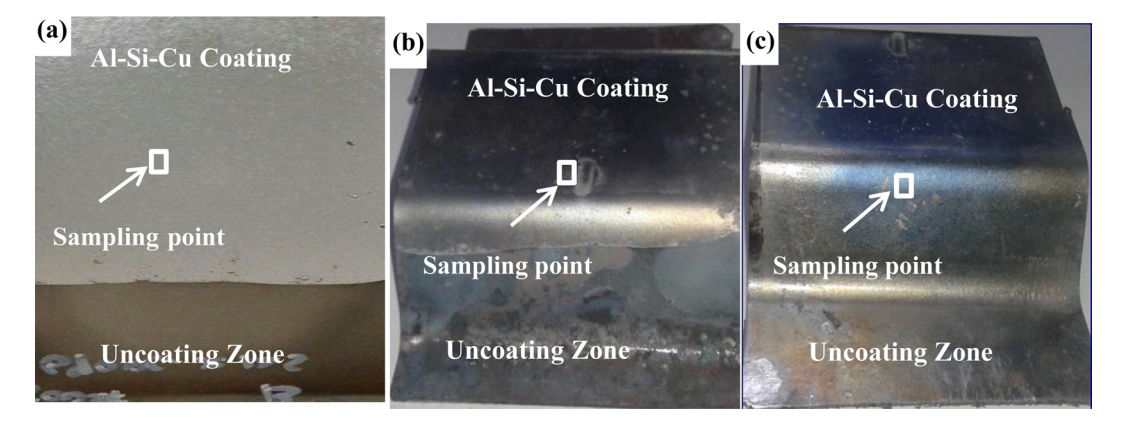


Figure 3: Morphology of coatings: (a) hot-dip coating, (b) hot stamping coating with forming radius of 2 mm, and (c) hot stamping coating with forming radius of 4 mm.

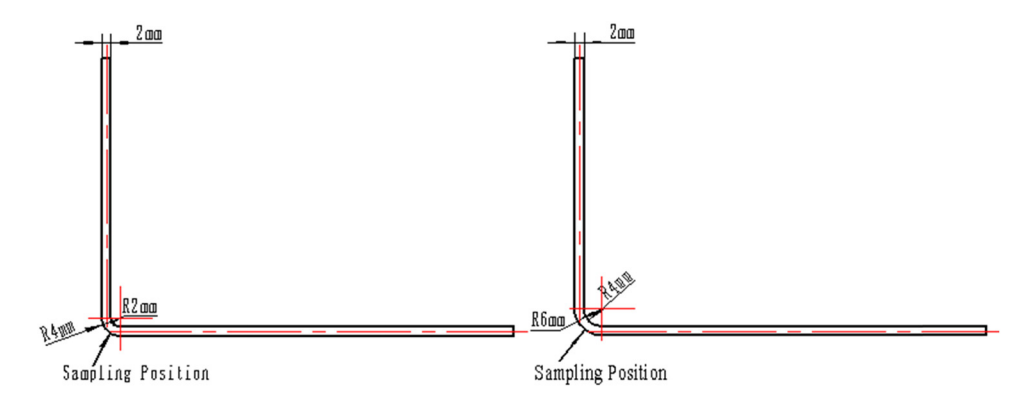


Figure 4: Pure bending schematic and sampling position of hot stamping coating.

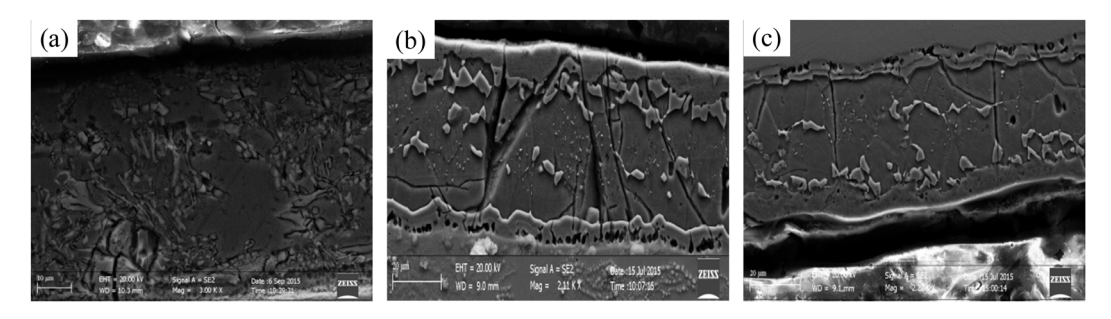
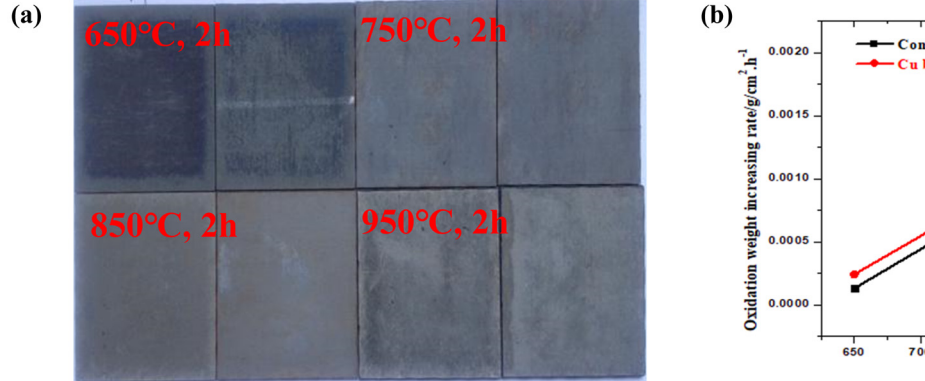


Figure 5: SEM micro-structure of coatings: (a) hot-dip coating, (b) hot stamping coating with forming radius of 2 mm, and (c) hot stamping coating with forming radius of 4 mm.

It can be seen that coating surfaces by different heating temperatures show uniform gray colors from dark gray to light gray and continuous and compacted outlooks. Uniform color distribution indicates that oxide distributions are uniform, and just little change of gray color indicates that oxide type do not change although the heating temperature reaching as high as 950°C. According to the study of Al–Si coating [6], the size of surface oxide

grain increases with the heating temperature increasing from 650 to 930°C and no microstructure type changes in this process.

Comparing with commercial Al–Si, oxidation weight increasing rate of Al–Si–Cu coatings also increases with the increasing heating temperature and especially has the same increasing slope from the heating temperature of 650 to 850°C and much slower increasing slope



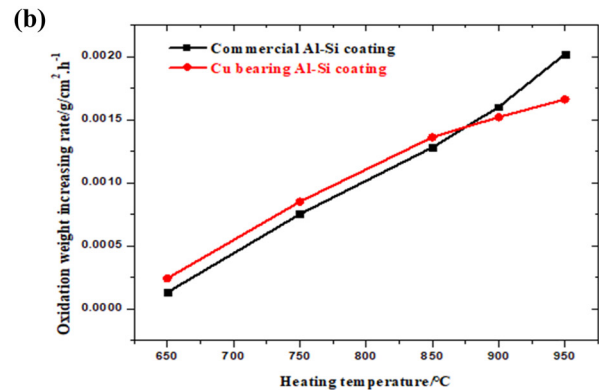


Figure 6: Surface morphology and oxidation weight increasing rate curve of Al-Si-Cu coating after heating with different temperatures:
(a) Al-Si-Cu coating surface morphology and (b) oxidation weight increasing rate curves.

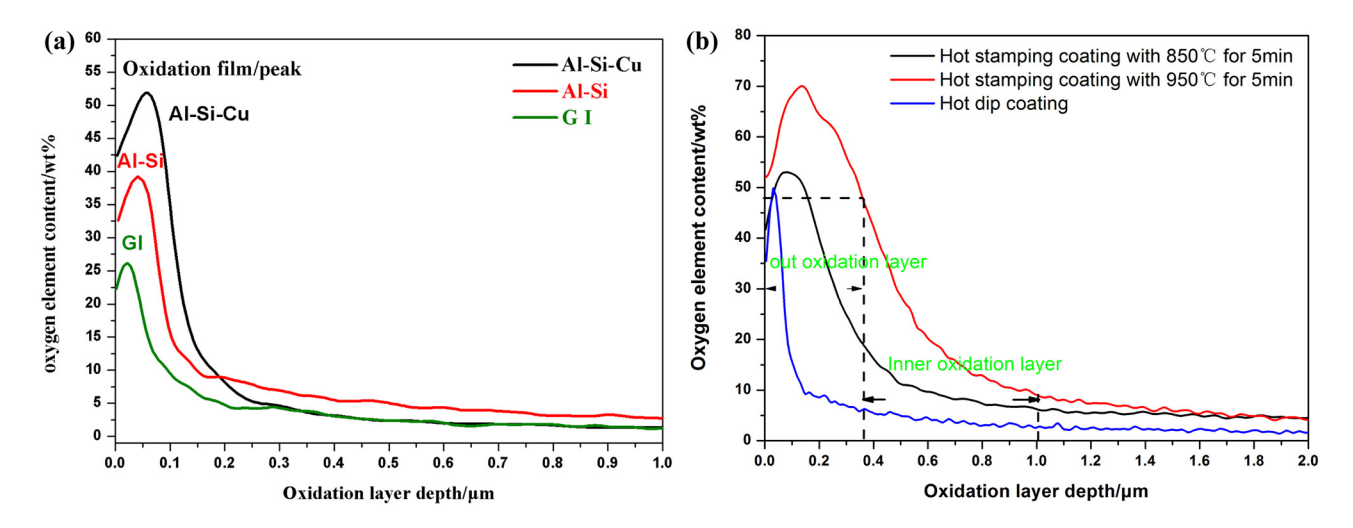


Figure 7: Oxygen element profiles of coatings: (a) different hot dip coatings and (b) Al-Si-Cu coatings after different hot stamping processes.

above 850°C. When the heating temperature is 850°C, the inflection points of the oxidation mass increase curves of the coatings appear. At the temperature of inflection point, the amount of oxidation weight increasing rate of Al–Si–Cu (0.00136 g·cm⁻²·h⁻¹) is slightly higher than that of Al–Si coating (0.00128 g·cm⁻²·h⁻¹). Figure 7 shows that Al–Si–Cu coating covers a bit high percentage of Al₂O₃ oxidation film that mainly leads to a little higher oxidation weight increase. Moreover, the perfect oxidation film means higher protective capability for coating and substrate steel [6,7], so Al–Si–Cu coating has higher high temperature oxidation resistance than Al–Si coating in this stage.

However, as heating temperature range from 850 to 950°C, microcracks appearing in Al–Si coating during the austenitizing treatment [6] result in an oxidation deterioration of coating and exposure of substrate. Hence, the oxidation weight increasing rate of Al–Si coating (0.00202 g·cm⁻²·h⁻¹) is much higher than that of Al–Si–Cu coating (0.00166 g·cm²·h⁻¹), which covers the continuous oxidation film (shown in Figures 5(b) and 7(a)) that could contain oxygen element transfer into inner coating or substrate steel.

The oxidation film thickness and oxygen content distribution of coating characterize oxidation properties. The perfect oxidation film with extent thickness can avoid oxygen atom permeating into inner coating. To futher evaluate oxidation film performance, oxygen element profile of different hot-dip coatings and hot forming coatings with heating temperature at 850 and 950°C is, respectively, shown in Figure 7(a) and (b). As shown in Figure 7(a) and Table 2, the thickness of oxidation film in Al–Si–Cu, Al–Si, and GI coatings is, respectively, 0.11, 0.082, and 0.044 μ m, and the average oxygen contents of oxidation film in Al–Si–Cu are, respectively, 47.15,

35.75, and 24.23 wt%. The thickness and oxygen content of oxidation film in Al–Si–Cu are obviously the highest value among these three coatings, which can give a perfect high-temperature protective ability to the coating. Approximately calculated by divided value of surface oxygen content in oxidation film and oxygen content of the corresponding metal oxide, the surface oxide percentage in oxidation film of three coatings is shown in Table 2. The average oxygen content of oxidation film in Al–Si–Cu coating is approximately equal to that in Al₂O₃ (oxygen content 47.06 wt%), so oxidation film of Al–Si–Cu can be evaluated as being composed of 100% Al₂O₃. However, Al–Si coating and GI coating are evaluated as being composed of 76% Al₂O₃ + 24% SiO₂, Fe₂O₃, tel., and 84.3% ZnO + 16.7% Al₂O₃, tel., respectively.

According to Table 2, Pilling-Bedworth ratio (PBR) of Al_2O_3 , SiO_2 , ZnO_3 and Fe_2O_3 is 1.28, 2.27, 1.59, and 4.29, respectively. On the basis of physical significance of PBR and study, when PBR \geq 1.00, the compressive stress develops in oxidation films, which can be estimated, integrated, and compacted [1,6]. The larger the difference between PBR and 1, the larger the growth stress. When PBR > 1.00, oxidation films fall off because of the excessive compressive stress [6]. Therefore, it can be concluded that oxidation films of Al-Si-Cu coating and Al-Si coating are integrated and compacted, and the oxidation film of GI coating will fall off in heating or hot stamping process. However, according to the oxidation film composition, only the oxidation film structure of Al-Si-Cu coating can be evaluated as 100% continual, integrated, and compacted. Al-Si coating and GI coating are mixtures of multiply oxidation structure containing majority oxide Al_2O_3 or ZnO + minority oxide SiO_2 or Fe_2O_3 .

Table 2: Parameters, composition, and compactness evaluation of oxidation film in different hot-dip coatings

Coating type	Average oxygen content of oxidation film (wt%)	Oxidation film thickness (µm)	Surface oxide composition in oxidation film	PBR	Compactness evaluation
Al-Si-Cu	47.15	0.110	100% Al ₂ O ₃	Al ₂ 0 ₃ :1.28	100% continual and compactness
Al-Si	35.75	0.082	76% Al ₂ O ₃ + 24% (SiO ₂ , tel.)	Al ₂ 0 ₃ :1.28	Mixture oxide
				SiO ₂ :2.27	
GI	24.23	0.044	84.3% ZnO + 16.7% (Al ₂ O ₃ , Fe ₂ O ₃ , tel.)	Zn0:1.59 Al ₂ 0 ₃ :1.28	Mixture oxide
				Fe ₂ 0 ₃ :4.29	

Table 3: Parameters, composition, and compactness evaluation of oxidation film in hot-dip and hot stamping Al-Si-Cu coatings

Coating type		Average oxygen content of oxidation film (wt%)	Oxidation film thickness (µm)	Surface oxide composition in oxidation film	Compactness evaluation
Hot dip Hot stamping coating	Heating temperature 850°C Heating temperature 950°C	44.9 47.35 61.5	0.082 0.204 0.266	95.4% $Al_2O_3 + 4.6\%$ (SiO ₂ , tel.) 100% Al_2O_3 with excess oxygen	Mixture oxide 100% continual and compactness Mixture oxide

Oxygen element profiles of hot-dipped and hot stamping Al-Si-Cu coatings with heating temperature 850 and 950°C are shown in Figure 7(b). Peaking oxygen contents of three profiles are 49.8, 53.0, and 70.0 wt%. It is calculated and shown in Table 3 that the average oxygen content of oxidation film of hot-dip and hot stamping coatings with the heating temperature of 850 and 950°C is 44.9, 47.35, and 61.5 wt%, and the thickness of oxidation film is 0.082, 0.204, and 0.266 µm, respectively. It can be seen that the oxidation film of hot stamping coating with the heating temperature of 850 and 950°C can be evaluated as being composed of 100% Al₂O₃ and 100% Al₂O₃ with excess oxygen, respectively. The average oxygen content and thickness of oxidation film increase with hot stamping and increasing heating temperature. However, the thickness of the whole oxidation layer (outer + inner) with the heating temperature of 950°C is still near 1.0 μm, which is almost the same as hot-dip and hot stamping coatings with the heating temperature of 850°C. Hence, it proves Al-Si-Cu coating can effectively inhibit oxygen diffusion to the inner coating and can explain why Al-Si-Cu coating does not have oxidation film scaling, failing in high-temperature heating, and hot stamping as shown in Figure 3(b) and (c).

The oxidation film thickness is defined in equation (2). Oxygen contents in different oxidation films are calculated by the average oxygen content from thickness 0 to $2 \times T_{\text{peaking}}$.

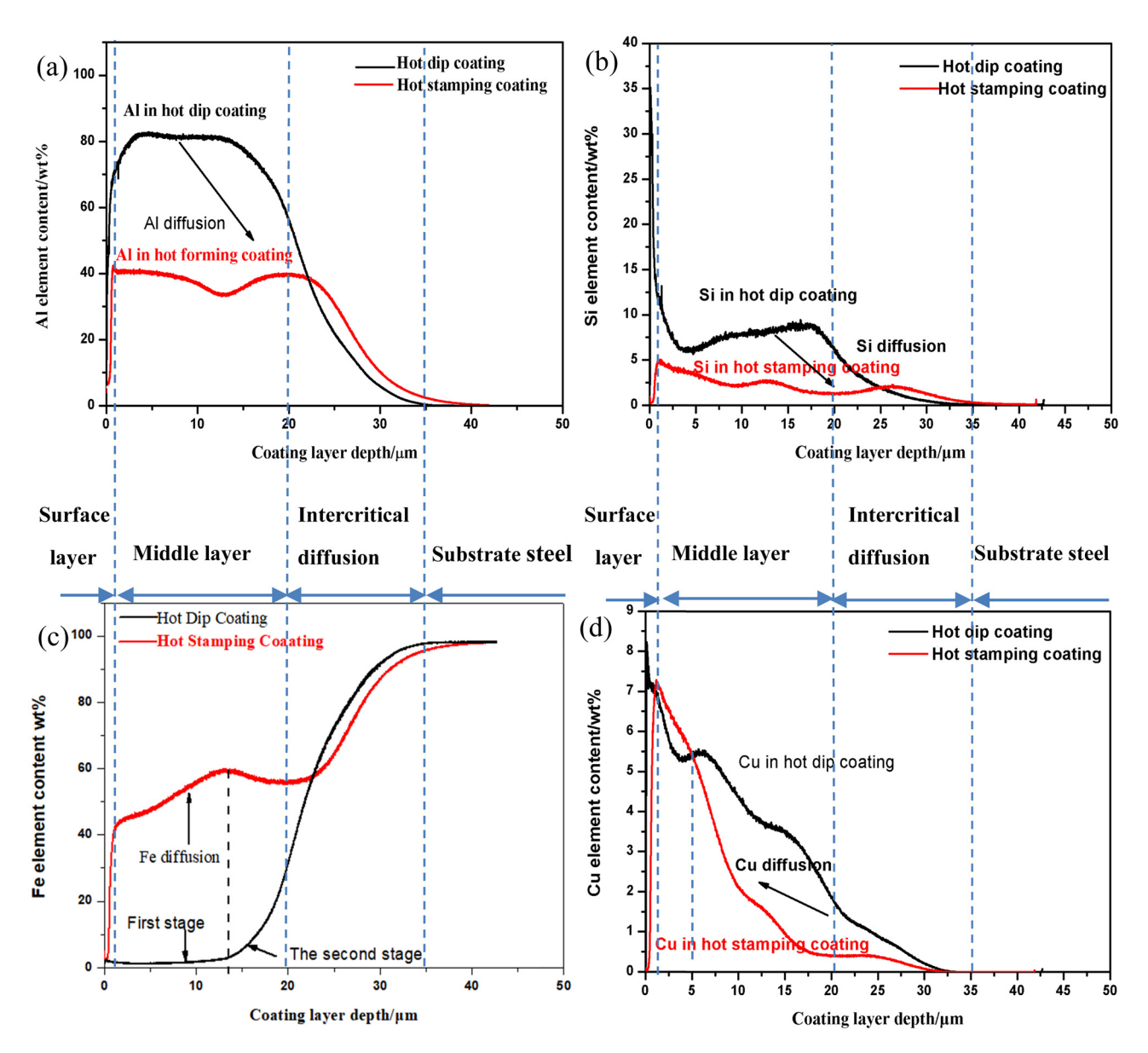


Figure 8: Element distribution in hot-dip and hot stamping coatings with the heating temperature of 850°C: (a) Al, (b) Si, (c) Fe, and (d) Cu.

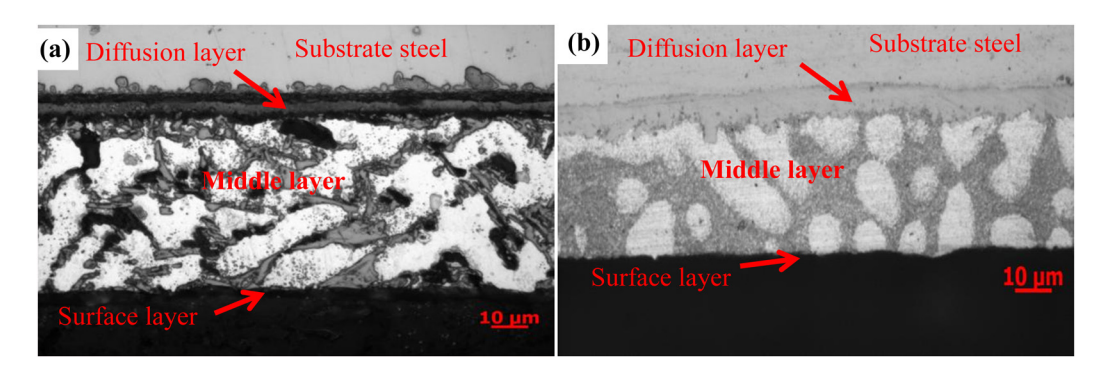


Figure 9: OM microstructure of coatings: (a) Al-Si-Cu coating and (b) Al-Si coating.

Table 4: Element content range in different layers of hot-dip and hot stamping coatings (wt%)

Coating type		Surfac	e layer			Middle	e layer			Diffus	ion layer	
	Al	Si	Fe	Cu	Al	Si	Fe	Cu	Al	Si	Fe	Cu
Hot dip Hot stamping	0-70 0-40	13-35 0-5	0-2 0-38	0-8.2 0-7.2	56-81 34-40	6-13 1.2-4.9	2-35 38-55	1.9-8.2 1.4-7.2	0-56 0-40	0-6 0-2.0	35-97 55-96	0-1.9 0-1.4

$$T_{\rm film} = T_{\rm peaking} \times 2$$
 (2)

In equation (1), $T_{\rm film}$ and $T_{\rm peaking}$, respectively, stand for thickness of oxidation film and peaking point of oxygen content.

The average oxygen content of oxidation films is specifically gained by integral calculation of oxygen element profiles from thickness 0 to $2 \times T_{\rm peaking}$ in Figure 7.

PBR values that stand for volume ratio of metal atom and its oxide in Table 2 are calculated by equation (3) [6]:

$$PBR = \frac{V_{ox}}{V_M} = (M \cdot d_0)/(n \cdot d_{ox} \cdot A)$$
 (3)

where M is molecular weight of oxide, d_0 is density of metal, n is number of metal atoms in molecular of oxide, d_{ox} is density of oxide, and A is metal atomic weight.

3.2.2 Element distribution of coating

Al, Si, Fe, and Cu element profiles of hot-dip and hot stamping coatings are shown in Figure 8. According to OM microstructure in Figure 9 and spot EDS value in Table 5, element distribution profiles are divided into surface layer, middle layer, intercritical layer, and substrate. As shown in Figure 8(a), Al content is relatively stable in the middle layer of coating and decreases smoothly in the intercritical layer with increasing depth. After hot stamping, the Al content decreases approximately 50% (from about 80–40 wt%) in the middle layer and increases a bit in the intercritical layer.

As shown in Figure 8(b), the Si content of hot-dip coating decreases from 35 to 13 wt% in the surface layer, alters from 6.0 to 13.0 wt% in the middle layer, and decreases from 6.0 to 0.0 wt% with increasing depth in the diffusion layer. It suggests that the Si element highly concentrates in the surface layer, stably fluctuates in the middle layer, steadily transfers to the substrate in the intercritical layer with an increasing depth. After hot stamping, the general distribution trend of the Si content does not change too much, whereas the Si content drastically reduces more than 61% in the surface layer and integrally decreases to about 30–50% in the middle layer.

As shown in Figure 8(c), the Fe content of hot-dip coating is less than 2 wt% in the surface layer, stably maintaining 2—3 wt% in the first stage of the middle layer

Table 5: Melting point of phases in Al-Si-Cu coating (°C)

Element/phase	Melting point (°C)
Al	660
Si	1,412
Cu	1,083
Al-10 wt% Si	577
FeAl ₃	1,157 [7]
FeAl	1,255 [16]
$Al_{15}Fe_3Si_2$	860 [8]
Al₅FeSi	870 [8]
Cu ₃ Al	1,049 [7]
Cu ₉ Al ₄	1,022 [9]

and smoothly increasing to 31 wt% in the second stage of the middle layer, and then steadily increasing to 92 wt% in intercritical layer with increasing depth. After hot stamping, the Fe content rapidly increases to 40 wt% in the surface layer, largely increases to relatively stable content (40–60 wt%) in the middle layer, and decreases a bit in the intercritical layer.

As shown in Figure 8(d), the Cu content in both hot-dip and hot stamping coating has almost the same distributing principle that it decreases with increasing depth. Segregation peaks of the Cu content profile in hot-dip and hot stamping coating are 8.22 and 7.2 wt%, respectively. After hot stamping, the Cu content profile is lower than that of hot-dip coating in surface layer, higher than that of hot-dip coating in the first stage of the middle layer, and lower than that of hot-dip coating in the second stage of the middle layer and intercritical layer.

As the analysis above, Al, Si, Fe, and Cu depth profiles have different distribution rules in both hot-dip and hot stamping coatings. Al and Si elements diffuse from the middle and intercritical layers to substrate steel. Fe diffuses from substrate steel to the middle layer, and Cu diffuses from the inner coating (the second stage of the middle layer + intercritical layer) to outer coating (the surface layer + the first stage of the middle layer) in the process of heating and hot stamping. It can be pointed out that different elements have different distribution characters, and that element diffusion in the process of hot dip, heating treatment, and hot stamping has greatly altered the element and phase composition of as-aluminized coating, as it was studied by Zhang et al. [7] and Sun et al. [8]. To further illustrate, the element content range in different layers of hot-dip and hot stamping coatings is summarized in Table 4. The distribution of Cu has a skin effect with a high content in the surface layer. As main binary elements in the coating, amounts of Al and Fe maintain balance. The Al-rich phase is distributed in the middle layer, the Fe-rich phase is distributed in the diffusion layer, the Si-rich phase is distributed in the surface layer [9–14]. After heating and hot stamping, the content of Al-rich and Si-rich phases decreases, and the content of Fe-rich phase increases in three layers of coating. These elements and phases have different physical properties including the melting point shown in Table 5 and hardness studied in the literature [15], which can greatly affect the high-temperature resistance and hot stamping ability.

The melting point of elementary substance phase or intermetacal phase of Si, Cu, FeAl₃, and Cu₃Al is 1,412, 1,083, 1,330, and 1,049°C, respectively, which is much higher than the melting point of Al-10 wt% Si (577°C)

Table 6: Microstructure feature of coating Al-Si-Cu and Al-Si coating

Coating type	Coating type Surface layer			Mid	Middle layer			Diffu	Diffusion layer
	Smoothness of		Metal compound	p		Rich Al phase		Thickness	Flatness of
	surface	Average width (µm)	Average length (μm)	Volume percent (%)	Average width (µm)	Average length (μm)	Volume percent (%)	uniformity	Interface
Al-Si-Cu Smooth	Smooth	4.29	21.49	42	7.91	20.25	58	Uniformity	Straight
Al-Si	Not smooth	9.32	10.34	67	7.05	11.56	51	Not uniformity	Not straight

and the temperature of hot stamping. Hence, these phases greatly enhance the melting point of coating and prevent coating softening and oxidation in the process of hot stamping. The melting point of ternary phase Al₁₅Fe₃Si₂ and Al₅FeSi is 860 and 870°C, respectively, which is higher than that of Al-10 wt% Si but very close to the temperature of hot stamping. Therefore, these phases should be carefully controlled with proper size and uniform distribution to avoid coating softening and oxidation in the process of hot stamping. The melting point of pure Al (660°C) is much lower than the temperature of hot stamping. But some Fe. Si. and Cu elements are dissolved in Al phase. which increases the melting point. At the same time, the hardness of Al solid solution phase (75 HV) is much lower than that of Fe₂SiAl₇ (1098 HV), FeAl (576 HV), and Fe₃Al (308 HV) [15], which proves Al phase has better hot forming ability. Hence, the phase composition of coating should be optimized to balance high-temperature oxidation resistance and hot forming ability. The following section will continue discussing this issue.

3.2.3 Microstructure of coatings

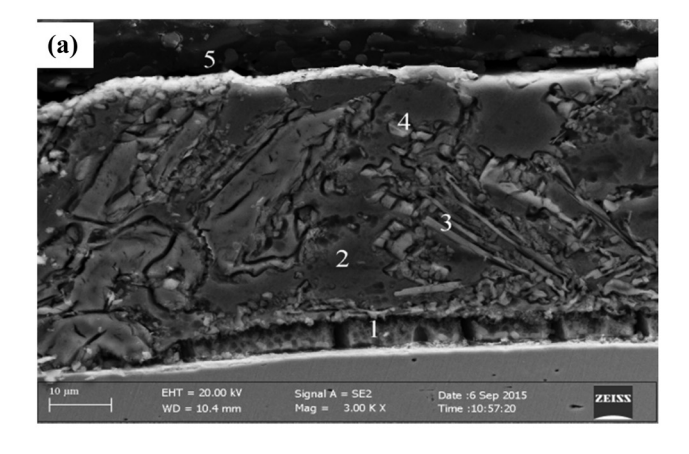
To further make clear the effects of microstructure on physical properties of Al–Si–Cu coating, OM microstructure of Al–Si–Cu coating and Al–Si coating is compared in Figure 9. Al–Si–Cu and Al–Si coatings are both composed of the surface layer, the middle layer, and the diffusion layer. The middle layer is composed of polygonal or nubbly the Al-rich phase with a white color and metal compound matrix with gray color in both coatings. Interface profiles of diffusion layer in Al–Si–Cu and Al–Si coatings are totally different; the former is straight and continual, and the latter is fluctuant and hackly. The

diffusion layer of Al–Si coating is composed of duck tongues protruding distributed in the middle layer.

Microstructure features including the phase dimension, phase percentage, and distribution of both coatings are obviously different, which are compared and listed in Table 6. It exhibits that the Al-Si-Cu coating has a smoother surface and straighter diffusion layer, longer and more narrow metal compound, and a bit higher content Al-rich phase comparing to Al-Si coating. In the middle layer of Al-Si-Cu coating, the average width and length of metal compound grains are 4.29 and 21.49 um, respectively, whereas the average width and length of Al-rich phase are 7.91 and 20.25 µm, respectively. The matrix metal compound uniformly embraces Al-rich phase, which exhibits skeleton structure. In the middle layer of Al-Si coating, the average width and length of metal compounds are 9.32 and 10.34 µm, respectively, whereas the average width and length of Al-rich phase are 7.05 and 11.56 µm, respectively. The Al-rich phase discretely is distributed in the matrix metal compound. The Al-Si-Cu coating has more uniform and finer microstructure than the Al-Si coating.

Phase structure and its element content tested by SEM and EDS are shown in Figure 10 and Table 7. Due to measuring range of EDS is about $1 \mu m$ thickness, the element content tested by EDS in the surface layer is a bit different from that tested by GDS in Figure 8 and Table 4.

The surface layer in both coatings is composed of aluminum oxide and Si-rich phase. In the surface layer of Al–Si–Cu coating, Cu is identified as an elementary substance phase with content of about 6.88%. Hence, Cu gives coating with high-temperature resistance and anticorrosion properties due to its high melting point and high-temperature resistance and anticorrosion properties itself.



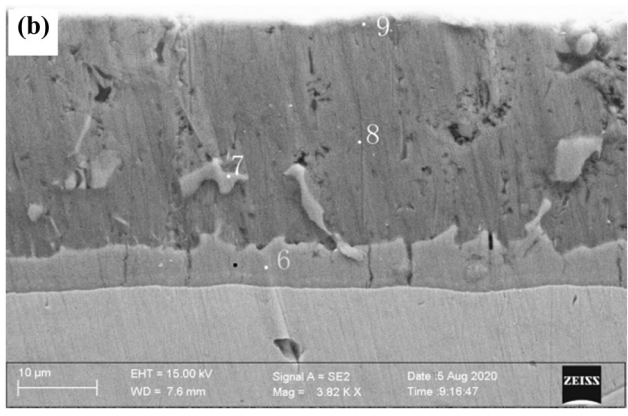


Figure 10: SEM microstructure and spot EDS position of coatings: (a) Al-Si-Cu coating and (b) Al-Si coating.

Table 7: EDS s	pot analysis of	hot-dip coatings	in Figure 10
----------------	-----------------	------------------	--------------

Coating type	EDS	spot position	Mass pe	rcentage (w	t%)			Phase
			Fe	Al	Si	Cu	0	
Al-Si-Cu	1	Diffusion layer	32.45	50.90	10.47	2.29	3.89	Al ₇ Fe ₂ Si, Al ₃ Fe, CuAl ₃
	2	Metal compound	2.45	60.21	28.37	3.69	5.28	Al−Si matrix, CuAl₃
	3	Metal compound	7.60	55.01	2.27	31.67	3.45	Al ₇ Fe ₂ Si, CuAl ₃
	4	Al-rich phase	1.11	89.26	1.86	2.90	4.87	Al matrix
	5	Surface layer	0.21	35.39	11.22	6.88	46.30	Al_2O_3 , Cu, Si-rich phase
Al-Si	6	Diffusion layer	30.45	51.45	11.88	_	6.22	Al ₇ Fe ₂ Si, Al ₃ Fe
	7	Metal compound	3.02	65.86	26.37	_	4.75	Al-Si matrix
	8	Al-rich phase	0.71	93.28	1.99	_	4.02	Al matrix
	9	Surface layer	2.41	48.80	12.58	_	36.21	Al ₂ O ₃ , Si-rich phase

The diffusion layer (points 1 and 7) in both coatings that have almost the same Al, Si, and Fe contents can be identified as Al₇SiFe₂ and Al₃Fe phases. About 2.29 wt% Cu dissolves in the diffusion layer, which is identified as CuAl₃. CuAl₃ formed in the process of solidification in hot dipping following the cooling section can suppress the diffusion layer uniformly growing and make coating with straight interface profile as shown in Figures 9(a) and 10(a). Hence, this can improve hot forming ability of the coating.

Al-rich phases (points 4 and 8) of both coatings are composed of α -Al (Al matrix) dissolving a small content of Fe and Si. In the Al–Si–Cu coating, 2.90 wt% Cu element bearing leads to solution strengthening and microstructure optimization (high volume, more uniform, wider, and longer dimension) of Al-rich phase as shown in Table 4 and obviously enhances the high-temperature resistance without decreasing the hot forming ability.

The types of metal compounds in the two coatings are different. Metal compounds (points 2 and 7) are composed

Fcc+Liquid
Beta_AlFeSi+Fcc+Liquid
Beta_AlFeSi+Diamond+Fcc+Liquid
Beta_AlFeSi+Diamond+Fcc

400
AlCu_Theta+Beta_AlFeSi+Diamond+Fcc

200
1 2 3 4 5
Cu / wt.%

Figure 11: Vertical section phase diagram of Al10Si0.4Fe-Cu system (FCC is Al, Diamond is Si, Beta_AlFeSi is $Al_9Fe_2Si_2$, and AlCu_Theta is Al_2Cu).

of the Al–Si matrix (containing the Al–Si–Fe phase) in both coatings. In the Al–Si–Cu coating, 3.69 wt% Cu can be identified as Cu_3Al . On account of high melting point of Cu_3Al (1,049°C), metal compounds of the Al–Si–Cu coating had a higher melting point than the Al–Si coating. Furthermore, as shown in Figure 6 and Table 4, metal compounds of Al–Si–Cu also have narrow width and skeleton structure, so it has a higher high-temperature resistance property.

To further clarify the effect of Cu addition on the phase separation of plating chromatography, the thermodynamic phase diagram containing Cu was calculated by Pandat software (BIS Group Technology Research Institute, Shanghai University, Technology Research Center and High Strength Automotive Steel Co., Ltd of HBIS Tang Steel). From the calculation results of Al10Si0.4Fe-Cu vertical section phase diagram (Figure 11), it can be seen that with the decrease in temperature, β -Al $_9$ Fe $_2$ Si $_2$ precipitates

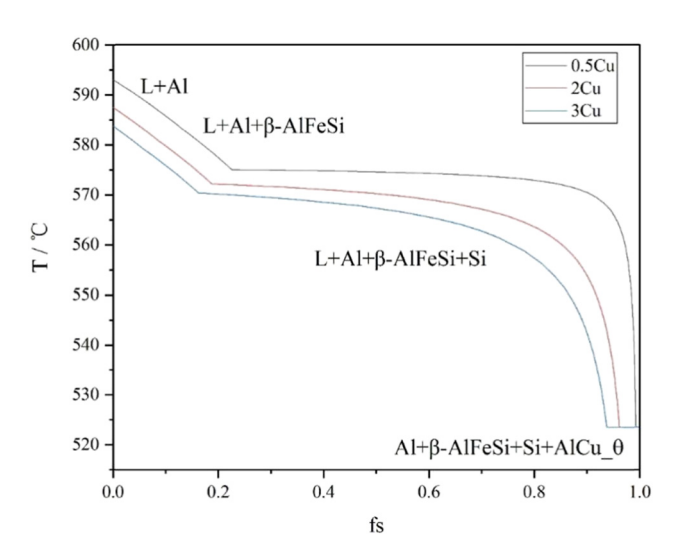


Figure 12: Calculation results of nonequilibrium solidification path of Al10Si0.4Fe-Cu system.

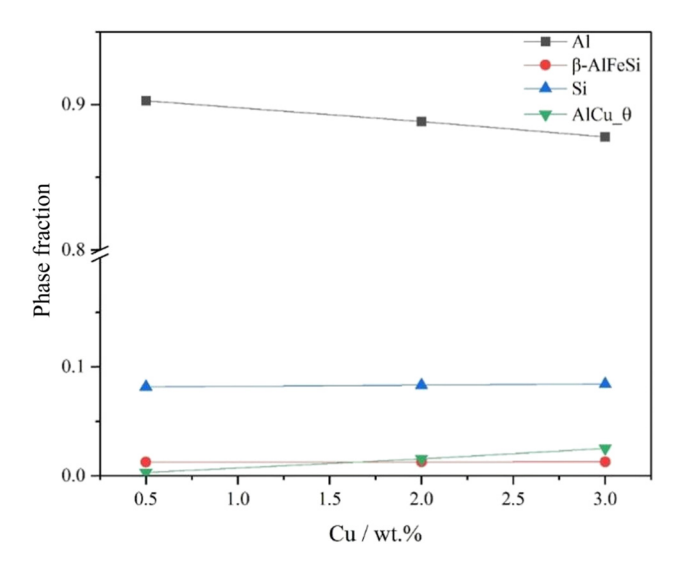


Figure 13: Phase fraction of alloy with different Cu contents after solidification.

first, and only this AlFeSi phase precipitates when the Cu content is less than 5 wt%. When the Cu content is between 0.5 and 3 wt%, the precipitation temperature of Al₂Cu increases and the Al₂Cu + Al₉Fe₂Si₂ + Si + Al phase region increases with the increase of Cu content, and the Al₂Cu + Al₉Fe₂Si₂ + Si + Al phase region changes from Al₉Fe₂Si₂ + Si + Al phase region. Therefore, with the increase of Cu content, Al₂Cu increases. The specific contents of precipitates can be obtained from the subsequent solidification path calculation results.

According to the unbalanced solidification path shown in Figures 12 and 13, Al10Si0.4Fe-0.5Cu starts to solidify at 593°C, and with the increase of Cu content, the melting point decreases, and the solidification termination temperature is about 523°C. Al appeared first, followed by Al₉Fe₂Si₂, followed by Si, and Al₂Cu only at the end of solidification. According to the phase fraction of the alloy with different Cu contents after solidification, with the increase of Cu content, the content of Al decreases, the content of Si and Al₂Cu increases to different degrees, whereas the content of Al₉Fe₂Si₂ is almost unchanged.

4 Conclusions

To enhance high-temperature resistance and hot forming ability of hot forming steel coating, a novel type of Al–Si–Cu coating features and their influence factors on high-temperature oxidation resistance and hot stamping ability were investigated. The main results of this study are summarized as follows:

- (1) Al-10% Si-(0.5–3.0%) Cu coating of 22MnB5 steel exhibits a balance of high-temperature resistance during 950°C heating and deep hot stamping ability without any cracks spreading into substrate steel as hot forming at 33.3% deformation strain.
- (2) Al-Si-Cu and Al-Si coatings have a very similar increasing slope of oxidation weight increasing rate between 650°C and 850°C, whereas above 850°C, the increasing slope of oxidation weight increasing rate curve of Al-Si-Cu is smaller than that of Al-Si coating.
- (3) Al–Si–Cu coating has a continual and compacting oxidation film structure. Al–Si and GI coatings have mixtures of multiple oxidation-containing majority oxide Al₂O₃/ZnO and minority oxide SiO₂/Fe₂O₃, respectively.
- (4) In hot-dip coating, the Si element highly concentrates in the surface layer, stably fluctuates in the middle layer, and steadily transfers to substrate steel in the intercritical layer with increasing depth. The distribution of Cu has a skin effect with peaking content of 8.2% in the surface layer. Al and Si elements diffuse from the middle and intercritical layers to substrate steel, Fe diffuses from substrate steel to the middle layer, and Cu diffuses from inner coating to outer coating after heating and hot stamping.
- (5) Al–Si–Cu coating has a smoother surface and straighter diffusion layer, longer and more narrow metal compound and a bit higher content-rich Al phase. The surface and diffusion layers are identified as aluminum oxide + Si-rich + Cu phase and Al₇SiFe₂ + Al₃Fe + CuAl₃, respectively. Al-rich phase and metal compound are composed of α-Al dissolving Fe, Si, and Cu as well as Al–Si matrix + Cu₃Al, respectively.

Funding information: This research was funded by Natural Science Foundation of Hebei Province in China (E2015318005) and HBIS Group Technology Research Institute (HG2016108).

Author contributions: Conceptualization and writing: Ziliu Xiong; methodology: Zhangguo Lin and Jianjun Qi; experiment: Li Sun and Guoping Zhou; date correction and precipitate simulation: Guangxin Wu and Shuang Kuang.

Conflict of interest: Authors state no conflict of interest.

References

[1] Berglund, G. The history of hardening of boron Steel in northern Sweden. 1st International Conference on Hot Sheet Metal Forming of High-Performance Steel, Kassel, Germany, 2008, pp. 176–177.

- [2] Tsuru, T. Hot-dipped Al-Mg-Si coating steel its structure, electrochemical and mechanical properties. *Corrosion Science and Technology*, Vol. 9, 2010, pp. 233–238.
- [3] Kruehong, C., G. A. EL-Mahdy, A. Nishikata, and T. Tsuru. Influence of second phases on the electrochemical behavior of hot dipped Al-Mg-Si coated steel. *Corrosion Science*, Vol. 52, 2010, pp. 2379–2386.
- [4] Takata, N., M. Nishimoto, S. Kobayashi, and M. Takeyama. Morphology and formation of Fe-Al intermetallic layers on iron hot-dipped in Al-Mg-Si alloy melt. *Intermetallics*, Vol. 54, 2014, pp. 136-142.
- [5] Zhang, J., S. M. Jiang, and Q. F. Zhang. Current status of coatings for hot formed steel. *Heat Treatment of Metals*, Vol. 40, No. 3, 2015, pp. 169–172.
- [6] Fan, D. W., H. S. Kim, J. K. Oh, K. G. Chin, and B. C. De Cooman. Coating degradation in hot press forming. *ISIJ International*, Vol. 50, No. 4, 2010, pp. 561–568.
- [7] Zhang, J., G. Wang, J. Shao, Y. Chen, and T. Yang. Pulverized coal combustion of nitrogen free blast furnace. *Journal of Iron* and Steel Research, Vol. 25, No. 6, 2013, pp. 1–6.
- [8] Zhang, Y., P. Zhu, and G. Chen. Lightweight design of automotive front side rail based on robust optimisation. *Thinwalled structures*, Vol. 45, No. 7–8, 2007, pp. 670–676.
- [9] Gui, Z. X., W. K. Liang, and Y. S. Zhang. Enhancing ductility of the Al-Si coating on hot stamping steel by controlling the Fe-Al

- phase transformation during austenitization. Science China Technological Sciences, Vol. 57, No. 9, 2014, pp. 1785–1793.
- [10] Lin, W., F. Li, D. Wu, X. Chen, X. Hua, and H. Pan. Effect of Al-Si coating on weld microstructure and properties of 22MnB5 steel joints for hot stamping. Journal of Materials Engineering and Performance, Vol. 27, No. 4, 2018, pp. 1825–1836.
- [11] Xiong, Z., Z. Lin, J. Qi, L. Sun, G. Wu, and S. Kuang. Cracking behavior of Al-Si coating on hot stamping boron steel sheet. *Procedia Engineering*, 2014, pp. 1713–1718.
- [12] Chunhua, X. and G. Wei. Pilling-Bedworth ratio for oxidation of alloys. *Material Research Innovations*, Vol. 3, 2000, pp. 231–235.
- [13] Guata, S. P. Intermetallic compound formation in Fe-Al-Si ternary system: Part I. *Materials Characterization*, Vol. 49, 2003, pp. 269-291.
- [14] Zhang, J., S. Jiang, Q. Zhang, and C. Liu. Effect of temperature on microstructure and formability of Al-10 mass% Si coatings. *Journal of Iron and Steel Research International*, Vol. 23, No. 3, 2016, pp. 270–275.
- [15] Grauer, S. J., E. J. F. R. Caron, N. L. Chester, M. A. Wells, and K. J. Daun. Investigation of melting in the Al-Si coating of a boron steel sheet by differential scanning calorimetry. *Journal of Materials Processing Technology*, Vol. 216, 2015, pp. 89-94.
- [16] Murray, J. L. The aluminium-copper system. *International Metals Reviews*, Vol. 30, 1985, pp. 211–233.